Hindawi Publishing Corporation
International Journal of Photoenergy
Volume 2014, Article ID 176965, 10 pages
http://dx.doi.org/10.1155/2014/176965

Research Article

Optical and Electrical Effects of p-Type μc-SiO$_x$:H in Thin-Film Silicon Solar Cells on Various Front Textures

Chao Zhang,[1] Matthias Meier,[1] Andreas Lambertz,[1] Vladimir Smirnov,[1] Bernhard Holländer,[2] Aad Gordijn,[1] and Tsvetelina Merdzhanova[1]

[1] *IEK5-Photovoltaik, Forschungszentrum Jülich, 52425 Jülich, Germany*
[2] *Peter Grünberg Institute (PGI-9), Forschungszentrum Jülich, 52425 Jülich, Germany*

Correspondence should be addressed to Chao Zhang; c.zhang@fz-juelich.de

Received 6 December 2013; Revised 12 March 2014; Accepted 12 March 2014; Published 14 April 2014

Academic Editor: Raghu N. Bhattacharya

p-type hydrogenated microcrystalline silicon oxide (μc-SiO$_x$:H) was developed and implemented as a contact layer in hydrogenated amorphous silicon (a-Si:H) single junction solar cells. Higher transparency, sufficient electrical conductivity, low ohmic contact to sputtered ZnO:Al, and tunable refractive index make p-type μc-SiO$_x$:H a promising alternative to the commonly used p-type hydrogenated microcrystalline silicon (μc-Si:H) contact layers. In this work, p-type μc-SiO$_x$:H layers were fabricated with a conductivity of up to 10^{-2} S/cm and a Raman crystallinity of above 60%. Furthermore, we present p-type μc-SiO$_x$:H films with a broad range of optical properties (2.1 eV $<$ band gap E_{04} $<$ 2.8 eV and 1.6 $<$ refractive index n $<$ 2.6). These properties can be tuned by adapting deposition parameters, for example, the CO_2/SiH_4 deposition gas ratio. A conversion efficiency improvement of a-Si:H solar cells is achieved by applying p-type μc-SiO$_x$:H contact layer compared to the standard p-type μc-Si:H contact layer. As another aspect, the influence of the front side texture on a-Si:H p-i-n solar cells with different p-type contact layers, μc-Si:H and μc-SiO$_x$:H, is investigated. Furthermore, we discuss the correlation between the decrease of V_{oc} and the cell surface area derived from AFM measurements.

1. Introduction

There has been a continuous interest in the development and application of hydrogenated microcrystalline silicon oxide (μc-SiO$_x$:H). It can be used as an intermediate reflector in thin-film silicon tandem solar cells containing a hydrogenated amorphous silicon (a-Si:H) top cell and a hydrogenated microcrystalline silicon (μc-Si:H) bottom cell connected in series, as reported in previous studies [1–5]. In this work, we focus on the development and application of p-type μc-SiO$_x$:H in thin-film silicon solar cells, that is, a mixed phase material containing a μc-Si:H and an amorphous silicon oxide (a-SiO$_x$:H) phase. These two phases result in a material with versatile properties. It has been proposed that the μc-Si:H phase provides high electrical conductivity, while the a-SiO$_x$:H phase improves the transparency and decreases the refractive index of the material [6]. Our state-of-the-art p-type layer stack, which is used in amorphous single junction or tandem solar cells fabricated on sputtered aluminum doped zinc oxides (ZnO:Al) front side TCO (transparent conductive oxide), included a p-type μc-Si:H contact layer. It provides a low resistive TCO/p contact, as discussed elsewhere [7–9], but causes an additional parasitic absorption; detailed examination is shown in reference [6, 10]. In order to overcome this issue, a p-type μc-SiO$_x$:H material with a high transparency and sufficient conductivity was developed [6, 11]. Moreover, it is reported that the refractive index n of p-type μc-SiO$_x$:H can be tuned in the broad range (2–3.5) [10]. Thus, this material is a promising candidate to be integrated as an antireflection layer between the front side TCO and the silicon solar cell.

In the present study, we report on the development of p-type microcrystalline silicon oxide material, fabricated by plasma enhanced chemical vapor deposition (PECVD), as single layer and its application in amorphous silicon single junction solar cells. Effects caused by variation of CO_2/SiH_4 ratio, layer thickness, and the dopant gas concentration are presented. In a second step, a-Si:H solar cells with two

Table 1: Overview of deposition parameters for the p-type μc-SiO_x:H layer deposition by PECVD.

Power density/W/cm^2	Frequency/MHz	Pressure/mbar	Temperature/°C	H_2 dil. (SiH_4:H_2)	r_{CO_2}	r_{TMB}
0.5	13.56	13.3	220	4.2 : 2000	1.2–6.0	0–0.036

different p-type contact layers (p-type μc-Si:H and p-type μc-SiO_x:H) were deposited on four different front side TCOs to investigate the influence of the surface texture on the solar cell's *IV*-characteristics, external quantum efficiency (EQE), and reflectance.

2. Experimental Details

We have deposited p-type μc-SiO_x:H layers with a thickness of several hundred nanometers by an RF-PECVD system (30 × 30 cm^2; 13.56 MHz), suitable for four 10 × 10 cm^2 substrates. The process gases used were silane (SiH_4), trimethylborane 2.54% ($B(CH_3)_3$-TMB) diluted in helium (He) from the company *Praxair,* and hydrogen (H_2) and carbon dioxide (CO_2) from the company *Linde*. They were applied to the process through a showerhead electrode. The electrode gap was 12.5 mm and the temperature during deposition was 220°C. *Corning Eagle XG* glass was used as substrates for the μc-SiO_x:H layer development. The deposition rate was about 1 Å/s. Development of p-type μc-SiO_x:H layers applied in solar cells was carried out on sputtered ZnO:Al as front TCO, which was wet-chemically etched in diluted hydrochloric acid (HCl) for texturing the materials surface: detailed investigations are shown elsewhere [12–14].

Commonly, we use the ratio between the CO_2-flow ϕ_{CO_2} and the SiH_4-flow ϕ_{SiH_4} defined as

$$r_{CO_2} = \frac{\phi_{CO_2}}{\phi_{SiH_4}}. \quad (1)$$

Likewise, we use the ratio between the TMB-flow ϕ_{TMB} and the SiH_4-flow ϕ_{SiH_4}:

$$r_{TMB} = \frac{\phi_{TMB}}{\phi_{SiH_4}}. \quad (2)$$

Because TMB is diluted (2.54% TMB in He), the net TMB-flow ϕ_{TMB} is only 2.54% of the value set for the mass flow controller. In the following, all gas flows are presented as net gas flows.

The oxygen content in the material was quantified by using Rutherford backscattering spectrometry (RBS) and is presented as the oxygen to silicon ratio $r_{O,RBS}$. Detailed experimental descriptions can be found in [15].

In order to produce material with a high crystalline volume fraction, the H_2 dilution (ratio between SiH_4- and H_2-flow) was kept at a constant ratio of 4.2 : 2000, while tuning the CO_2- or TMB-flow in the PECVD process. For variations done for the CO_2/SiH_4 ratio r_{CO_2}, the TMB/SiH_4 ratio r_{TMB} was set at 0.005. For variations done for r_{TMB}, the CO_2/SiH_4 ratio was set at 2.4. An overview of the deposition parameters is given in Table 1.

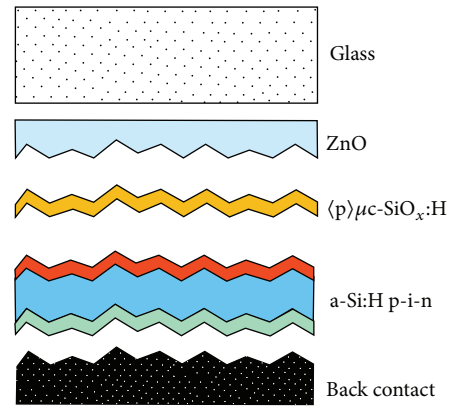

Figure 1: Scheme of an a-Si:H solar cell in p-i-n configuration containing p-type μc-SiO_x:H as a window layer.

Figure 1 shows a scheme of a hydrogenated amorphous thin-film silicon (a-Si:H) solar cell with intergraded p-type μc-SiO_x:H as a contact layer at the ZnO/Si interface instead of a p-type μc-Si:H contact layer. Solar cells were deposited with a variation in thickness and TMB-flow for the p-type μc-SiO_x:H layer. For the thickness variation, the r_{CO_2} was 2.4 and for r_{TMB} was 0.0014.

We used photothermal deflection spectroscopy (PDS) as a highly sensitive tool for the investigation of optical absorption [16]. The setup consists of a cavity filled with CCl_4 which surrounds the sample. A monochromatic chopped light beam illuminates the sample in a wavelength range of 310 nm < λ < 2600 nm. The heat generation in the sample due to absorption and the heat transfer to the surrounding fluid cause a change of the refractive index of CCl_4 which is detected by a passing laser beam. The band gap E_{04} is defined as the photon energy at which the absorption coefficient α is 10^4 cm^{-1}. The refractive indices n ($n_{1000\,nm}$) at a wavelength of λ = 1000 nm have been calculated from reflection and transmission measurements using the Fresnel equation, described in more detail in [3]. The electrical conductivity was measured in planar direction. For the estimation of the crystalline volume fraction (I_c), Raman spectroscopy (λ = 488 nm) was used [17]. For I_c, the ratio between the integrated peak signal at 520 cm^{-1} to the total integral (a-SiO_x:H and μc-Si:H) was calculated [3]. For *IV*-measurements under AM 1.5 illumination a double source sun simulator (class-A) was used. In all cases, an average value of the best three solar cells of one sample containing 18 cells (10 × 10 mm^2 each) was used. The external quantum efficiency (EQE) measurements were carried out by a monochromatic chopped probe beam with 10 nm resolution in a wavelength range from 300 to 800 nm.

Table 2: Overview of front TCOs and applied procedures; autocorrelation length (ACL) and root mean square (RMS) roughness are presented as a measure of surface texture.

Type	Front TCO	1st treatment	2nd treatment	ACL/nm	RMS/nm
A	ZnO:Al	40 s HCl	—	715	110
B	ZnO:Al	20 s HF	5 s HCl	490	85
C	ZnO:Al	30 s HCl	10 s HF	630	125
D	SnO_2:F (AsahiU)	50 nm ZnO:Al protection layer		195	40

To investigate the influence of the front side TCO texture on the solar cell performance and light management, a-Si:H solar cells with p-type μc-Si:H or p-type μc-SiO_x:H as a contact layer were deposited. An overview of the front side TCOs can be found in Table 2. Three types of etching procedures were applied to the sputtered ZnO:Al containing HCl etched (type A), firstly HF and subsequently HCl (type B) [18] and firstly HCl and subsequently HF etched ZnO:Al (type C) [19]. A concentration of 0.5 wt% for HCl and of 1 wt% for HF was used. As a comparison to a commercially available front TCO, Asahi type U SnO_2:F (type D), covered by a 50 nm thick ZnO:Al layer for protection reasons against reduction due to the hydrogen plasma, was also used.

The different TCOs were imaged by scanning electron microscopy (SEM). The surface topographies and characteristic feature sizes were measured and statistically analyzed by atomic force microscopy (AFM, NanoStation 300, SIS). The root mean square (RMS) roughness and the autocorrelation length (ACL), which describes the lateral size of a surface structure, are taken as a measure.

3. Results

3.1. p-Type μc-SiO_x:H Material Development. Figure 2(a) shows the conductivity σ as a function of the band gap E_{04} for p-type μc-SiO_x:H. A broad range of E_{04} and σ can be achieved with variation of the CO_2 gas flow, as indicated at the top of the graph. By increasing CO_2/SiH_4 ratio r_{CO_2} from 1.2 to 6, the band gap increases from 2.2 to 2.8 eV. In the course of this parameter variation, the refractive index n decreases from 2.6 to 1.6, as shown in Figure 2(b). Also, the conductivity drops from 1.6×10^{-2} to 2×10^{-12} S/cm by increasing r_{CO_2}. From literature, it is known that window layers for solar cell applications should have a conductivity of $>10^{-6}$ S/cm when prepared as several hundred nanometer thick single layer on glass [20]. This limit is shown by the dashed line in Figures 2(a) and 2(b).

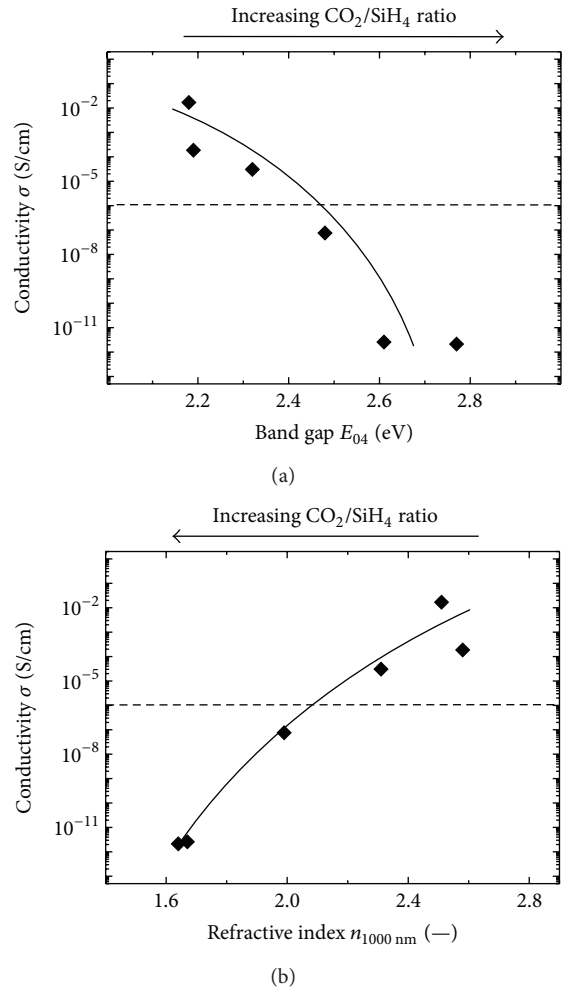

Figure 2: (a) Conductivity σ as a function of band gap energy E_{04} for various μc-SiO_x:H thin films. (b) Conductivity σ as a function of refractive index $n_{1000\,nm}$. Dashed lines mark the required conductivity for a solar cell device aiming at a high FF. The increase in CO_2/SiH_4 ratio is indicated by an arrow at the top of the graph.

Figure 3(a) shows the oxygen/silicon ratio measured by RBS $r_{O,RBS}$ as a function of the CO_2/SiH_4-ratio r_{CO_2}. A linear dependency between both values within the investigated range can be seen. Figure 3(b) shows the electrical conductivity σ and Raman crystallinity I_c of p-type μc-SiO_x:H as a function of r_{CO_2} and versus r_{TMB} in Figure 4. To provide a sufficient conductivity of the p-type μc-SiO_x:H, a certain crystalline volume fraction is required, as reported in [4, 11]. The crystalline volume fraction I_c of the p-type μc-SiO_x:H material is between 39% and 48% for an r_{CO_2} from 1.2 to 3.6. The maximum of I_c is at an $r_{CO_2} = 2.4$. For an r_{CO_2} higher than 3.6, the crystalline volume fraction is almost zero. This drop in σ coincides with the decrease of the Raman intensity ratio I_c. Furthermore, it is observed that with higher r_{CO_2}, the value for conductivity decreases from 1.7×10^{-2} S/cm to 10^{-12} S/cm which is close to the detection limit of the measurement system. For the (later) application in solar cells, a p-type μc-SiO_x:H material with an oxygen/silicon ratio of 0.5 was used.

Another important process parameter for the development of p-type μc-SiO_x:H is the TMB gas flow, which is

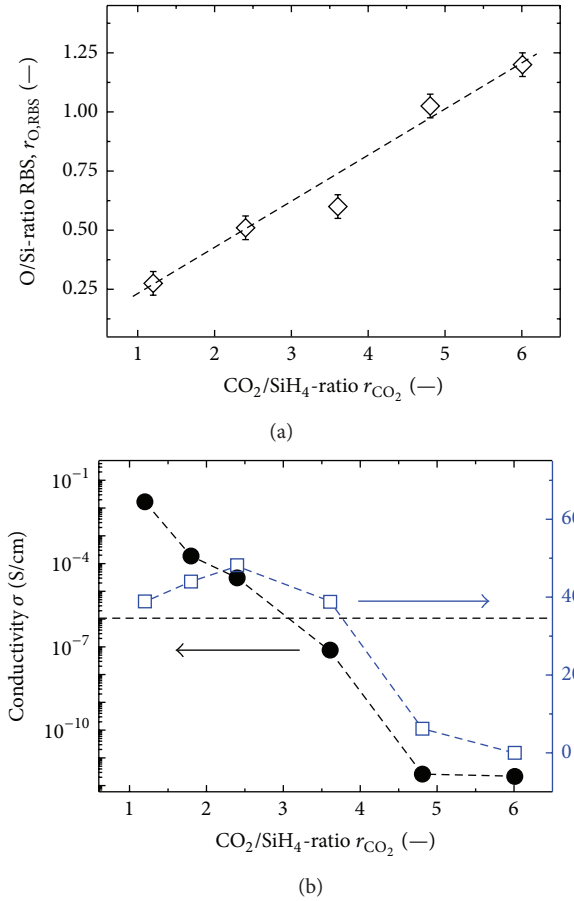

FIGURE 3: (a) Oxygen/silicon ratio measured using RBS. (b) Conductivity σ and Raman intensity ratio I_c of p-type μc-SiO_x:H layer as a function of CO_2/SiH_4-ratio. The dashed line in (b) marks the required conductivity for a solar cell device with high FF. The dashed line in (a) is a guide to the eye.

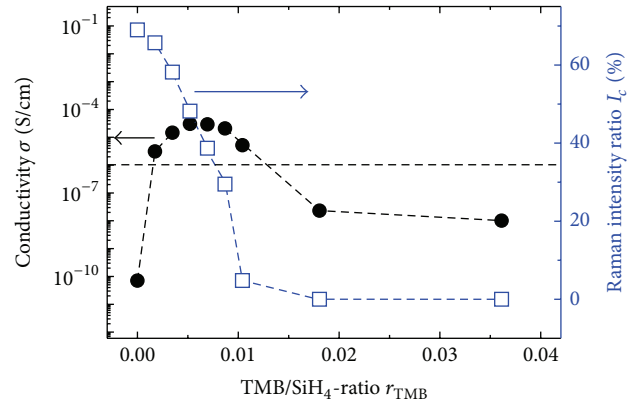

FIGURE 4: Conductivity σ and Raman intensity ratio I_c as a function of TMB/SiH_4-ratio r_{TMB}. The dashed line is a guide to the eye.

the dopant gas source. Figure 4 shows a sharp decrease of the crystalline volume fraction I_c from 69% to 5% caused by a slight increase of r_{TMB} from 0 to 0.01. For higher r_{TMB} values the material becomes fully amorphous. From this figure, it is also apparent that the conductivity of the material is in the range of 1×10^{-10} S/cm when no dopant was added. With a little admixture of TMB ($r_{TMB} = 0.002$), the conductivity increases to 3×10^{-6} S/cm. The maximum of σ is found for $r_{TMB} = 0.005$ at $\sigma = 3 \times 10^{-5}$ S/cm. For values, $r_{TMB} < 0.005$, a TMB admixture improves the conductivity due to an increase in the dopant concentration, whereas a further increase of TMB leads to the opposite effect due to the reduced crystalline volume fraction. For fully amorphous materials the conductivity remains at a level of around 10^{-8} S/cm.

3.2. Implementation of p-Type μc-SiO_x:H Contact Layers to Solar Cells. Figure 5 shows *IV*-curves of a-Si:H solar cells with varied thicknesses of p-type μc-SiO_x:H layers (2 nm to 8 nm). The solar cells are deposited on an HCl etched ZnO:Al (type A). The layer thickness was calculated from the deposition rate of 1 Å/s. The reference solar cell with a p-type μc-Si:H contact layer and a solar cell without contact layer, that is, only a p-type a-SiC:H layer, are also shown here. The applied p-type μc-SiO_x:H contact layers have a band gap of 2.3 eV, a refractive index of 2.3, and a conductivity of 3×10^{-5} S/cm. The reference solar cell with a p-type μc-Si:H contact layer has a fill factor of 69.2%. For the a-Si:H cell without contact layer, an "S-" shape of the *IV*-curve is observed resulting in a FF of only 59.6%. p-type μc-SiO_x:H layers of different thicknesses were used to replace p-type μc-Si:H; see Figure 1. Clear differences regarding the FF can be seen here. Increasing the thickness of the p-type μc-SiO_x:H layer from 2 nm to 8 nm results in an improvement of the fill factor of the a-Si:H cell by 12% (FF = 69.1%). The open circuit voltage V_{oc} of solar cells with p-type μc-SiO_x:H layers (0.93 V) is similar to solar cells with a p-type μc-Si:H contact layer. Solar cells without a contact layer have a V_{oc} of only 0.79 V.

In Figure 6, the corresponding external quantum efficiency EQE spectra of a-Si:H solar cells with a p-type μc-Si:H contact layer (reference), p-type μc-SiO_x:H contact layer of different thicknesses, and without a contact layer are presented. Particularly, in the short wavelength range some differences between various layer stacks are evident. The a-Si:H solar cells without contact layer reveal the highest EQE, while, for the reference solar cell, the EQE is reduced in the wavelength range between 320 and 600 nm. The quantum efficiency in this wavelength range of the solar cells with a 2 nm thick p-type μc-SiO_x:H layer is higher in comparison to the reference. However, the EQE decreases with increasing μc-SiO_x:H layer thickness. From the absorptance curves, it is seen that no decrease in cell reflection was achieved in the wavelength range between 350 and 550 nm by implementing a μc-SiO_x:H window layer with those applied thicknesses.

In Figure 7, the photovoltaic parameters (η, FF, V_{oc}, J_{sc}) of solar cells with p-type μc-SiO_x:H as window layer with TMB/SiH_4 ratio r_{TMB} varying from 0.0017 to 0.0052 are presented. The most pronounced effects are seen in the fill factor, shown in Figure 7(b). For the solar cell with a TMB/SiH_4 ratio of 0.0035, a maximum in FF was found. Also, for the V_{oc}, a maximum at the same r_{TMB} is seen in

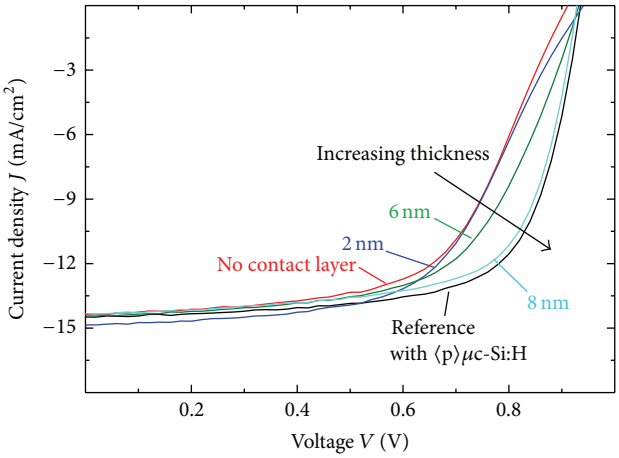

Solar cell	FF (%)
No contact layer	59.6
2 nm μc-SiO$_x$:H	57.1
6 nm μc-SiO$_x$:H	60.3
8 nm μc-SiO$_x$:H	69.1
Reference	69.2

FIGURE 5: IV-curves of a-Si:H solar cells under illumination with p-type μc-SiO$_x$:H contact layer of different thicknesses varying from 2 nm to 8 nm. For comparison, an a-Si:H solar cell with p-type μc-Si:H contact layer (indicated as reference) and an a-Si:H solar cell without any additional contact layers are shown.

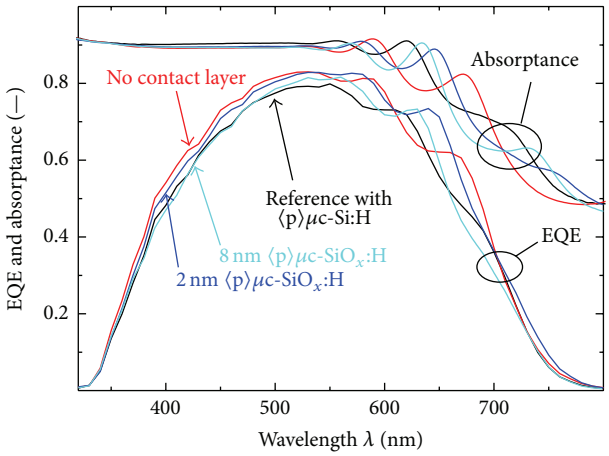

FIGURE 6: External quantum efficiency (EQE) and absorptance of a-Si:H solar cells without contact layer, that is, only p-type a-SiC:H layer; with p-type μc-Si:H contact layer (indicated as reference); with p-type μc-SiO$_x$:H contact layer (2 nm and 8 nm thick). All solar cells are deposited on type A ZnO:Al.

Figure 7(c). Both effects result in a slight improvement in efficiency compared to the reference solar cell, Figure 7(a). J_{sc} decreases slightly with increasing r_{TMB} (Figure 7(d)).

3.3. Investigations of a-Si:H Solar Cells on Various Front TCOs. SEM images of different front TCOs (details given in Table 2) are shown in Figure 8. The various surface topographies differ in terms of structure type (crater or pyramid), structure size, and steepness. These front side TCOs are ZnO:Al with large and flat craters (type A), ZnO:Al with smaller and steeper craters (type B), double textured ZnO:Al with a primarily large crater structure containing a secondary structure consisting of much smaller and steeper craters (type C), and Asahi type U SnO_2:F with its typical pyramid-like surface texture (type D).

The photovoltaic parameters of a-Si:H solar cells deposited on different front TCOs with a p-type μc-Si:H as well as with a p-type μc-SiO$_x$:H as a contact layer are presented in Figure 9. The p-type μc-SiO$_x$:H layer was deposited with a TMB/SiH_4 ratio of 0.0035, a CO_2/SiH_4 ratio of 2.4, and a thickness of 8 nm. It is shown that a-Si:H solar cells with a p-type μc-Si:H contact layer (displayed as triangles in Figure 9) on type A and type C ZnO:Al have an efficiency of around 9.4%. Solar cells deposited on type-B ZnO:Al with small and steeper craters show an enhanced efficiency of 9.9% which is in the same range of solar cells deposited on Asahi type U SnO_2:F. It is apparent that the short-circuit current density J_{sc}, fill factor (FF), and open circuit voltage V_{oc} show large variance for solar cells deposited on different surface textures. For solar cells deposited on types A and C TCO, the short-circuit current density J_{sc} is 14.8 mA/cm^2. Solar cells deposited on types B and D front TCO show a higher J_{sc} of 15.2 mA/cm^2 and 15.0 mA/cm^2, respectively. A reduced fill factor was observed on a solar cell deposited on TCO type A (67%), while the FF remains at about 70% for solar cells deposited on top of TCOs types B, C, and D. Larger differences can be observed in V_{oc}. Solar cells deposited for types A and B ZnO:Al show a V_{oc} of 0.935 V. For solar cells deposited on type C ZnO:Al, the V_{oc} is reduced by 0.03 V.

In a further step, the same series of different front TCOs were used for deposition of a-Si:H solar cells with a p-type μc-SiO$_x$:H layer as a contact layer (shown as circles in Figure 9). Generally the same trends for the different front TCOs are seen with those cells. The application of μc-SiO$_x$:H as a p-layer is suitable for ZnO:Al and it is not suited for Asahi type U SnO_2:F, even though it is covered by a thin ZnO:Al protection layer. This combination led to a significant drop of FF and J_{sc}. Also, the V_{oc} was reduced. To conclude, the introduction of p-type μc-SiO$_x$:H resulted in a reduction of efficiency of absolute 2%, when it was deposited on type D front TCO. The highest J_{sc} (15.4 mA/cm^2) was achieved with

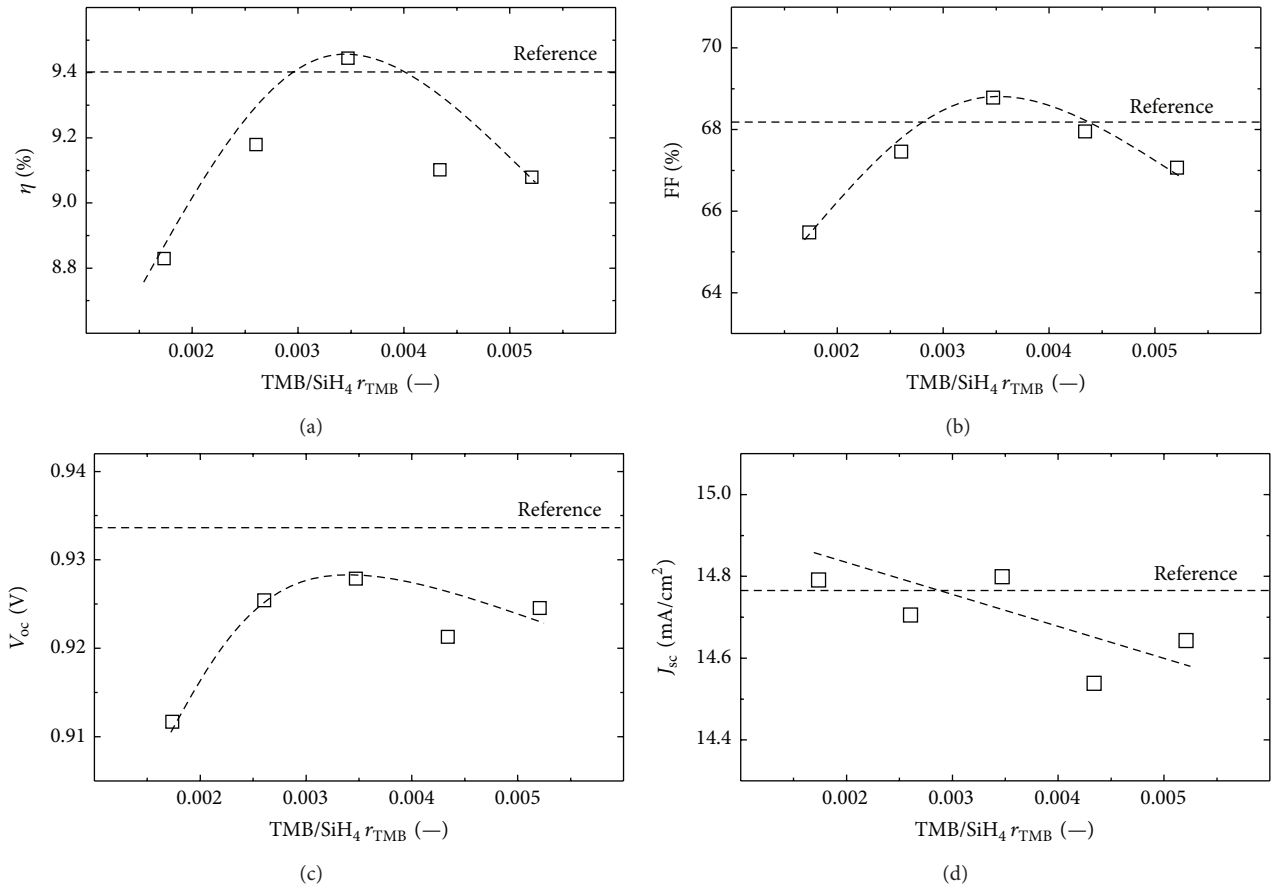

FIGURE 7: (a) Efficiency η, (b) fill factor FF, (c) open circuit voltage V_{oc} and (d) short-circuit current density J_{sc} of a-Si:H solar cells with p-type μc-SiO$_x$:H as window layer with various TMB/SiH$_4$ ratio r_{TMB}; the reference is an a-Si:H solar cell with p-type μc-Si:H as a contact layer. The dashed lines are guides to the eye.

a solar cell deposited on type B (firstly HF and subsequently HCl etched) ZnO:Al with a p-type μc-SiO$_x$:H.

In Figure 10, EQE measurements are presented to take a closer look to the optical effects given by different front TCOs as discussed in detail before. The EQE spectra show a-Si:H solar cells with p-type μc-SiO$_x$:H as a contact layer.

Beside the difference in the absorption edge of the two different TCO materials ZnO:Al (types A to C) and SnO$_2$:F (type D), clear differences regarding light management between differently treated ZnO:Al are seen. The EQE measurements approve the short-circuit current density presented in Figure 9. Furthermore, differences with respect of interference fringes visible in the long wavelength range can be observed. More precisely, it is apparent that after the single treatment with HCl as well as for the small features of Asahi type U SnO$_2$:F interferences remain and cause a noticeable loss in the long wavelength range compared to solar cells deposited on double etched ZnO:Al. Those interferences are reduced for solar cells deposited on either type B or type C ZnO:Al. The light incoupling is enhanced significantly and the reflection loss is reduced. Same trends are seen for solar cells with a p-type μc-Si:H contact layer, not shown here.

4. Discussion and Summary

In the present work, we were able to tune the band gap of p-type hydrogenated microcrystalline silicon oxide from 2.2 to 2.8 eV by increasing the CO$_2$/SiH$_4$ ratio r_{CO_2} from 1.2 to 6. But at the same time, while improving the optical transparency the electrical conductivity dropped. A low conductive material cannot be applied in a solar cell device without significant loss of performance and it is apparent that there is a tradeoff between transparency and electrical conductivity. Therefore, r_{CO_2} has to be chosen in a way resulting in a wider band gap for a higher transparency, a relatively low refractive index, and at the same time a sufficient electrical conductivity. It is seen that, for p-type μc-SiO$_x$:H, prepared in this study, a CO$_2$/SiH$_4$ ratio of 2.4 ($r_{O,RBS}$ = 0.5) or lower is crucial for applications in a solar cell. Besides, the oxygen content in the mixed phase material reduces its crystallinity from an r_{CO_2} > 2.4.

On the other hand, a strong influence on I_c is seen in Figure 4 for the variation of r_{TMB}. In that case, the amount of dopant sensitively affects the material's electrical conductivity. To be more precise, a certain amount of TMB is needed, whereas too much of it corrupts the material's crystallinity and with that the electrical conductivity. Therefore,

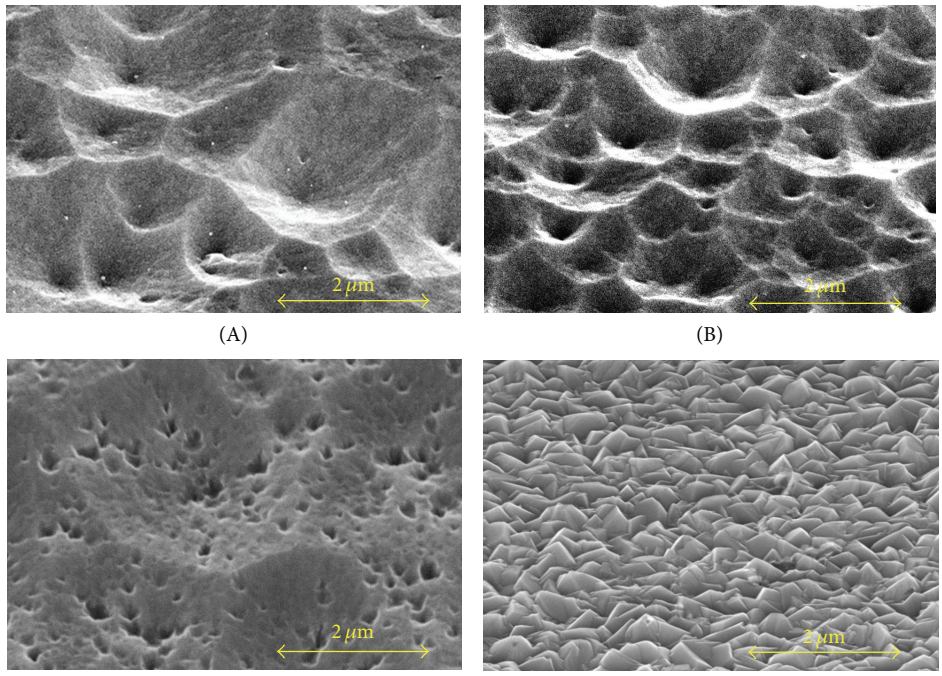

Figure 8: SEM images of front TCOs described in Table 2. Type A: HCl etched ZnO:Al with large craters, type B: HF and HCl etched ZnO:Al with small and steeper craters, type C: HCl and HF etched ZnO:Al with large and small crater features (double texture), and type D: Asahi type U SnO_2:F pyramid-like surface topography.

an optimized dopant concentration is essential to provide an adequate conductivity.

The same findings are confirmed by a series of solar cell results where r_{TMB} for the p-type μc-SiO_x:H layer was varied in small ranges (see Figure 7). Here, it is shown that the optimum for the TMB/SiH_4 ratio resulted in an improvement of fill factor and therefore in an improvement of conversion efficiency. Another important finding was that not only the composition of process gases but also the thickness of the p-type μc-SiO_x:H affects the FF strongly, as shown in Figure 5. The results reveal that a certain thickness is essential for a low resistive ohmic contact between ZnO:Al and the p-layer. However, thicker layers lead to additional absorptions (Figure 6) and increased series resistance. Though a reduced absorption within the contact layer, achieved by replacing a p-type μc-Si:H layer with a more transparent p-type μc-SiO_x:H, could be achieved, it can be concluded that finding a well-balanced contact layer thickness is essential for a high conversion efficiency of a solar cell.

Investigations of a-Si:H solar cells deposited on various front textures point out differences in terms of electrical and optical properties. Regarding the short-circuit current of a-Si:H solar cells, good performances are achieved for type B and type D front side TCOs. This is driven by the, particularly for a-Si:H solar cells, highly suitable light scattering provided by those textures. Particularly for type B TCO, which contains smaller and steeper crater structures in comparison to type A TCO an improved J_{sc} is observed. From the results of the EQE measurement, an enhanced light incoupling is approved. Also, the solar cell reflection is reduced over the complete wavelength range. For type C TCO (HCl and HF etched ZnO:Al), a decreased V_{oc} of about 30 mV is measured. This could be a cause of the typical crater structure created by the wet chemical etching step with hydrofluoric acid [21]. It is supposed that the small and steep features in the front texture lead to a loss in open circuit voltage. However, no correlation between autocorrelation length or *RMS* roughness and V_{oc} can be seen. But what can be observed is a correlation between the V_{oc} and the surface area of different front side TCOs. Each surface area can be calculated from AFM data. The normalized surface area A_{norm} (surface area of a nontextured ZnO:Al is defined as $1\,cm^2$) is displayed as a function of the V_{oc} (Figure 11). It is shown that with larger surface areas a decrease in V_{oc} occurs. A possible explanation for that coherence is an enhanced surface recombination between electrons and holes at the larger TCO/p-layer interface area. Other publications associate the decrease of V_{oc} with the formation of cracks and an enhanced recombination in the bulk material [22].

The application of μc-SiO_x:H as a p-layer on top of various front contacts leads to different observations. In Figure 9(d), it is seen that the μc-SiO_x:H layer improves the short-circuit current of solar cells deposited on type B TCO in contrast to other front textures. A reason for that might be the good light incoupling texture consisting of smaller craters (ACL 490 nm). It is possible that the improved light incoupling is additionally enhanced by the low refractive index and low absorption of p-type μc-SiO_x:H layer. In the case of type D TCO (SnO_2:F Asahi type U), p-type μc-SiO_x:H causes a strong decrease of FF and J_{sc}. An explanation could be that

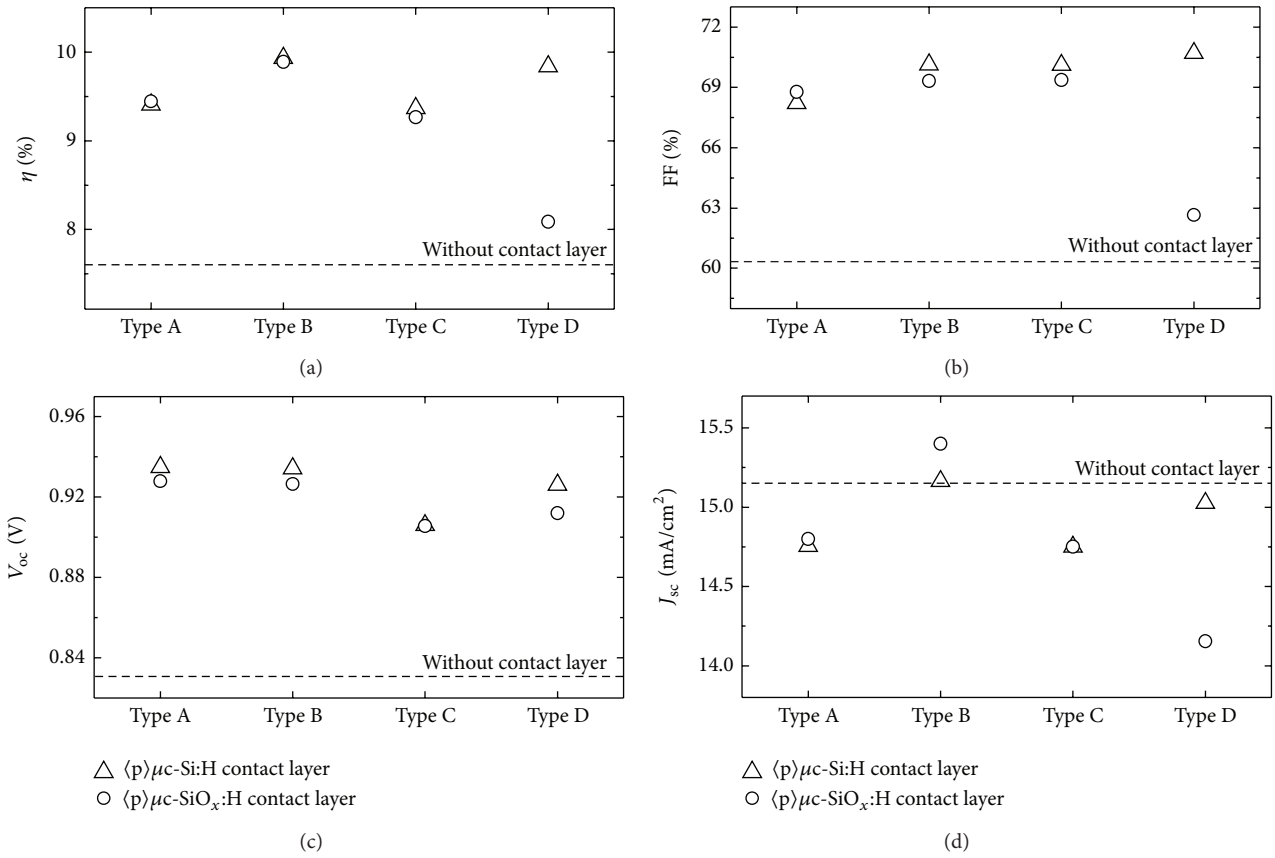

FIGURE 9: (a) Efficiency η, (b) fill factor (FF), (c) open circuit voltage V_{oc}, and (d) short-circuit current density J_{sc} of a-Si:H solar cells with p-type μc-Si:H (triangles) and p-type μc-SiO$_x$:H (circles) deposited on various front TCOs consisting of type A (HCl etched ZnO:Al); type B (first HCl subsequently HF etched ZnO:Al); type C (first HF subsequently HCl etched ZnO:Al); and type D (Asahi type U SnO_2:F). The dashed line represents solar cell characteristics of an a-Si:H solar cell without any contact layer, that is, only a p-type a-SiC:H layer.

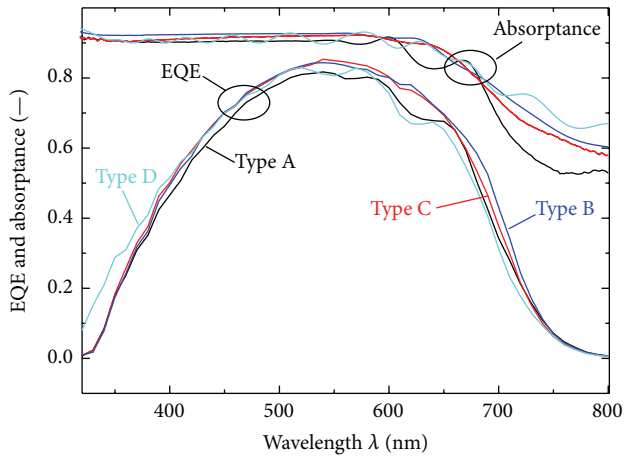

FIGURE 10: External quantum efficiency (EQE) and the absorptance of a-Si:H cell deposited on various types of front TCOs with p-type μc-SiO$_x$:H as a contact layer.

the combination of high power density, high H_2 dilution, and high deposition pressure used for deposition of the p-type μc-SiO$_x$:H caused a reduction of SnO_2:F front contact even though it is covered by a thin ZnO:Al layer for protection. It has been reported that hydrogen plasma can cause formation of elementary Sn and SiO_2 which result in high absorption and a reduction of fill factor in solar cells [7, 23]. For all front textures, a lower V_{oc} is observed when a p-type μc-SiO$_x$:H layer was used as a contact layer instead of a p-type μc-Si:H layer. A possible explanation for this might be that the p-type μc-SiO$_x$:H has an insufficient doping. However, an increased TMB-flow would not lead to a better result since, as seen in Figures 4 and 7, a higher amount of the dopant would cause a decrease of crystallinity which will again negatively influence the fill factor.

5. Conclusions

In this work, we have studied material characteristics like electrical conductivity, band gap, and refractive index of p-type μc-SiO$_x$:H and how they change by using different deposition parameters. As key attributes of a player to provide adequate electrical properties, p-type μc-SiO$_x$:H layers were fabricated with a conductivity up to more than 10^{-2} S/cm and a Raman crystallinity of over 60%. It is seen that there is a tradeoff between transparency and electrical conductivity. The optical properties of p-type μc-SiO$_x$:H can be tuned over

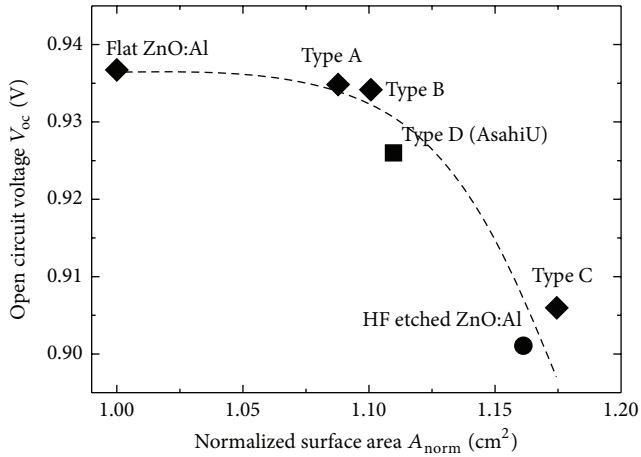

FIGURE 11: Open circuit voltage V_{oc} of a-Si:H solar as a function of the normalized surface area of different front TCOs. The surface area of a flat ZnO:Al is defined as 1 cm^2. The dashed line is a guide to the eye.

a broad range (2.1 eV < E_{04} < 2.8 eV and $n_{1000\,nm}$ down to 1.6) by adapting deposition parameters like CO_2/SiH_4 ratio in the gas mixture. These material properties are similar to the previous findings for n-type μc-SiO_x:H material [2, 3].

The photovoltaic parameters of the fabricated a-Si:H solar cells show that sensitive changes in layer thickness and also in the amount of the dopant TMB cause large effects on the fill factor. Slightly higher conversion efficiencies were achieved by implementing p-type μc-SiO_x:H.

Different front side TCO materials and surface textures have been investigated and compared. They show clear differences with respect to V_{oc} and J_{sc}. A correlation between the V_{oc} and the surface area of the front side TCO, calculated from AFM measurements, has been observed. It is seen that a larger surface area leads to a decrease of V_{oc}. An explanation is given by an enhanced surface recombination at the larger TCO/p-layer interface area. Moreover, similar trends are seen for the two different contact layers p-type μc-Si:H and p-type μc-SiO_x:H. The best result (η = 9.9%) was found on ZnO:Al with small and steeper craters for both types of p-doped layers. That means that an efficiency improvement of absolutely 0.5% was achieved in comparison to the reference solar cell deposited on only HCl etched ZnO:Al.

Conflict of Interests

The authors declare that there is no conflict of interests regarding the publication of this paper.

Acknowledgments

The authors would like to thank J. Kirchhoff, U. Gerhards, G. Schöpe, A. Bauer, M. Ghosh, M. Hülsbeck, S. Tillmanns, and O. Thimm. They thank U. Rau for his continuous support and encouragement. This work was carried out in the framework of the FP7 Project "Fast Track," funded by the EC under Grant Agreement no. 283501.

References

[1] P. Buehlmann, J. Bailat, D. Domié et al., "In situ silicon oxide based intermediate reflector for thin-film silicon micromorph solar cells," *Applied Physics Letters*, vol. 91, no. 14, Article ID 143505, 2007.

[2] T. Grundler, A. Lambertz, and F. Finger, "N-type hydrogenated amorphous silicon oxide containing a microcrystalline silicon phase as an intermediate reflector in silicon thin film solar cells," *Physica Status Solidi C: Current Topics in Solid State Physics*, vol. 7, no. 3-4, pp. 1085–1088, 2010.

[3] A. Lambertz, T. Grundler, and F. Finger, "Hydrogenated amorphous silicon oxide containing a microcrystalline silicon phase and usage as an intermediate reflector in thin-film silicon solar cells," *Journal of Applied Physics*, vol. 109, no. 11, Article ID 113109, 2011.

[4] V. Smirnov, A. Lambertz, B. Grootoonk, R. Carius, and F. Finger, "Microcrystalline silicon oxide (μc-SiO_x:H) alloys: a versatile material for application in thin film silicon single and tandem junction solar cells," *Journal of Non-Crystalline Solids*, vol. 358, no. 17, pp. 1954–1957, 2012.

[5] A. Lambertz, V. Smirnov, T. Merdzhanova et al., "Microcrystalline silicon-oxygen alloys for application in silicon solar cells and modules," *Solar Energy Materials and Solar Cells*, vol. 119, pp. 134–143, 2013.

[6] P. Cuony, M. Marending, D. T. L. Alexander et al., "Mixed-phase p-type silicon oxide containing silicon nanocrystals and its role in thin-film silicon solar cells," *Applied Physics Letters*, vol. 97, no. 21, Article ID 213502, 2010.

[7] M. Kubon, E. Böhmer, F. Siebke, B. Rech, C. Beneking, and H. Wagner, "Solution of the ZnO/p contact problem in a-Si:H solar cells," *Solar Energy Materials and Solar Cells*, vol. 41-42, pp. 485–492, 1996.

[8] B. Rech and H. Wagner, "Potential of amorphous silicon for solar cells," *Applied Physics A: Materials Science & Processing*, vol. 69, no. 2, pp. 155–167, 1999.

[9] J. Müller, O. Kluth, S. Wieder et al., "Development of highly efficient thin film silicon solar cells on texture-etched zinc oxide-coated glass substrates," *Solar Energy Materials and Solar Cells*, vol. 66, no. 1–4, pp. 275–281, 2001.

[10] K. Schwanitz, S. Klein, T. Stolley, M. Rohde, D. Severin, and R. Trassl, "Anti-reflective microcrystalline silicon oxide p-layer for thin-film silicon solar cells on ZnO," *Solar Energy Materials and Solar Cells*, vol. 105, pp. 187–191, 2012.

[11] A. Lambertz, F. Finger, B. Holländer, J. K. Rath, and R. E. I. Schropp, "Boron-doped hydrogenated microcrystalline silicon oxide (μc-SiO_x:H) for application in thin-film silicon solar cells," *Journal of Non-Crystalline Solids*, vol. 358, no. 17, pp. 1962–1965, 2012.

[12] O. Kluth, B. Rech, L. Houben et al., "Texture etched ZnO:Al coated glass substrates for silicon based thin film solar cells," *Thin Solid Films*, vol. 351, no. 1-2, pp. 247–253, 1999.

[13] M. Berginski, J. Hüpkes, M. Schulte et al., "The effect of front ZnO:Al surface texture and optical transparency on efficient light trapping in silicon thin-film solar cells," *Journal of Applied Physics*, vol. 101, no. 7, Article ID 074903, 2007.

[14] W. Böttler, V. Smirnov, J. Hüpkes, and F. Finger, "Texture-etched ZnO as a versatile base for optical back reflectors with well-designed surface morphologies for application in thin film solar cells," *Physica Status Solidi A*, vol. 209, no. 6, pp. 1144–1149, 2012.

[15] B. Holländer, H. Heer, M. Wagener, H. Hailing, and S. Mantl, "New high-precision 5-axes RBS/channeling goniometer for ion

beam analysis of 150 mm Ø wafers," *Nuclear Instruments and Methods in Physics Research B: Beam Interactions with Materials and Atoms*, vol. 161–163, pp. 227–230, 2000.

[16] W. B. Jackson, N. M. Amer, A. C. Boccara, and D. Fournier, "Photothermal deflection spectroscopy and detection," *Applied Optics*, vol. 20, no. 8, pp. 1333–1344, 1981.

[17] C. Smit, R. A. C. M. M. van Swaaij, H. Donker, A. M. H. N. Petit, W. M. M. Kessels, and M. C. M. van de Sanden, "Determining the material structure of microcrystalline silicon from Raman spectra," *Journal of Applied Physics*, vol. 94, no. 5, pp. 3582–3588, 2003.

[18] H. Zhu, J. Hüpkes, E. Bunte, J. Owen, and S. M. Huang, "Novel etching method on high rate ZnO:Al thin films reactively sputtered from dual tube metallic targets for silicon-based solar cells," *Solar Energy Materials and Solar Cells*, vol. 95, no. 3, pp. 964–968, 2011.

[19] J. Hüpkes, J. I. Owen, E. Bunte et al., "New texture etching of zinc oxide: tunable light trapping for Si thin film solar cells," in *Proceedings of the 25th European Photovoltaic Solar Energy Conference*, pp. 3224–3227, Valencia, Spain, 2010.

[20] B. Rech, *Solarzellen aus amorphem silizium mit hohem stabilem wirkungsgrad: zum einfluss des p/i-Grenzflächenbereichs und der intrinsischen absorberschicht [thesis-RWTH]*, Forschungszentrum Jülich, Zentralbibliothek, Forschungszentrum Jülich, Institut für Schicht-und lonentechnik, Aachen, Germany, 1997.

[21] J. I. Owen, J. Hüpkes, H. Zhu, E. Bunte, and S. E. Pust, "Novel etch process to tune crater size on magnetron sputtered ZnO:Al," *Physica Status Solidi A: Applications and Materials Science*, vol. 208, no. 1, pp. 109–113, 2011.

[22] H. Sakai, T. Yoshida, T. Hama, and Y. Ichikawa, "Effects of surface morphology of transparent electrode on the open-circuit voltage in a-Si:H solar cells," *Japanese Journal of Applied Physics*, vol. 29, no. 4, pp. 630–635, 1990.

[23] H. Schade, Z. E. Smith, J. H. Thomas III, and A. Catalano, "Hydrogen plasma interactions with tin oxide surfaces," *Thin Solid Films*, vol. 117, no. 2, pp. 149–155, 1984.